The Journal of Chemical Physics

RAPID COMMUNICATION | JULY 24 2023

Ultrafast transient vibrational action spectroscopy of cryogenically cooled ions

Special Collection: 2023 JCP Emerging Investigators Special Collection

Liangyi Chen ; Zifan Ma; Joseph A. Fournier

J. Chem. Phys. 159, 041101 (2023)
https://doi.org/10.1063/5.0155490

The Journal of Chemical Physics COMMUNICATION pubs.aip.org/aip/jcp

Ultrafast transient vibrational action spectroscopy of cryogenically cooled ions

Cite as: J. Chem. Phys. 159, 041101 (2023); doi: 10.1063/5.0155490
Submitted: 20 April 2023 • Accepted: 25 May 2023 •
Published Online: 24 July 2023

Liangyi Chen, Zifan Ma, and Joseph A. Fournier[a)]

AFFILIATIONS

Department of Chemistry, Washington University in St. Louis, St. Louis, Missouri 63130, USA

Note: This paper is part of the 2023 JCP Emerging Investigators Special Collection.
[a)]**Author to whom correspondence should be addressed:** jfournier@wustl.edu

ABSTRACT

Ultrafast transient vibrational action spectra of cryogenically cooled $Re(CO)_3(CH_3CN)_3^+$ ions are presented. Nonlinear spectra were collected in the time domain by monitoring the photodissociation of a weakly bound N_2 messenger tag as a function of delay times and phases between a set of three infrared pulses. Frequency-resolved spectra in the carbonyl stretch region show relatively strong bleaching signals that oscillate at the difference frequency between the two observed vibrational features as a function of the pump–probe waiting time. This observation is consistent with the presence of nonlinear pathways resulting from underlying cross-peak signals between the coupled symmetric–asymmetric C≡O stretch pair. The successful demonstration of frequency-resolved ultrafast transient vibrational action spectroscopy of dilute molecular ion ensembles provides an exciting, new framework for the study of molecular dynamics in isolated, complex molecular ion systems.

I. INTRODUCTION

Ultrafast coherent multidimensional spectroscopies have become invaluable techniques to interrogate molecular structures, interactions, and dynamics in the condensed phase spanning the THz to x-ray regimes.[1–7] Spectroscopic studies of increasingly complex chemical and biological systems present many challenges in data collection and, in particular, data analysis and interpretation. These challenges include spectral congestion, signal overlap, solvent background, solute–solvent interactions, and the need for high concentrations. In an effort to overcome these challenges, significant recent advances have been made in the collection of ultrafast nonlinear spectra in isolated gas-phase systems.[8–16] The low number densities of dilute gas-phase ensembles, however, often prohibit the ability to directly measure light absorption and the emitted nonlinear signal field. Instead, indirect "action" approaches that encode the desired nonlinear signals are required, which present unique technical challenges.

Early seminal work in action-based experiments by Marcus demonstrated the acquisition of transient and two-dimensional electronic spectra of Rb vapor by monitoring modulations in the fluorescence signal as a function of the pulse delay times.[17,18] More recently, Brixner reported 2D electronic action spectra of neutral species in the gas phase generated in molecular beams and detected with mass spectrometry via photoionization.[19,20] Stienkemeier has likewise measured 2D electronic action spectra via photoionization of neutral gas-phase species using He nanodroplet techniques.[21,22] In related studies, Allison has directly measured the electronic transient absorption spectra of neutrals produced in molecular beams using cavity enhancement and frequency-comb laser sources.[23,24] Collectively, this impressive, growing volume of studies is opening new avenues for unraveling fundamental molecular interactions and dynamics.

While time-resolved photofragmentation signals have been measured on gaseous molecular ions to track reaction kinetics[25,26] and excited-state lifetimes,[27] frequency-resolved action-based ultrafast spectroscopies of isolated molecular ions have yet to be demonstrated. The extension of ultrafast nonlinear spectroscopies to molecular ions is highly desirable, as well-established mass spectrometric techniques can be used to precisely generate, manipulate, and composition-select the desired chemical species of interest. Furthermore, soft ionization methods allow for the isolation of more diverse chemical and biological systems, providing more direct comparisons to condensed-phase studies. The very low density ($<10^6$ cm^{-3}) of ions that can be stored, however, makes the detection of time-domain modulations in weak nonlinear signals a grand challenge to overcome. Toward this goal, we recently demonstrated the collection of linear cryogenic ion vibrational spectra[28] using an ultrafast

IR pulse pair by monitoring the photodissociation of a weakly bound N_2 messenger "tag" molecule.[29–33] The Fourier transform of the time-domain tag-loss interferogram, which was derived from interferences in the excited vibrational coherences, yielded the linear frequency-domain spectrum. We also demonstrated the presence of detectable nonlinear signal but did not frequency-resolve the response.

Herein, we present the acquisition of ultrafast nonlinear vibrational action spectroscopy on cryogenically cooled, dilute molecular ion ensembles. Using a pulse shaper to control the ultrafast pulse sequence and isolate the desired nonlinear signal, we observe relatively strong bleaching signals in the C≡O stretch region of the metal-carbonyl complex *fac*-$Re(CO)_3(CH_3CN)_3^+$ tagged with a single N_2 molecule. Importantly, the carbonyl bleaching signals oscillate with pump–probe waiting time, with a period corresponding to the energy difference between the excited vibrational features, consistent with coherent coupling between the vibrational modes. With this successful demonstration, we provide the framework needed to collect multidimensional IR spectra and transient UV/Vis-IR spectra of charged molecular systems.

II. EXPERIMENTAL DETAILS

A detailed description of the cryogenic ion photofragmentation mass spectrometer, laser pulse generation, data acquisition, and data processing is provided in the supplementary material.

III. RESULTS AND DISCUSSION

An overview of the linear vibrational action spectrum of $Re(CO)_3(CH_3CN)_3^+ \cdot N_2$ in the carbonyl stretching region is presented in Fig. 1. The N_2 tag-loss action response was monitored as a function of the delay time τ between an IR pulse pair [Fig. 1(a)]. The tag-loss interferogram is shown in Fig. 1(b), which was undersampled using a 1700 cm^{-1} rotating frame (i.e., the phase difference between the two pulses, $\Delta\phi_{12}$, was incremented by $\omega_{1700}\tau$). Rotating frame sampling greatly reduced the number of points and, therefore, the time required to collect each interferogram. The interferogram shows a clear beating pattern expected from absorption at two frequencies, and the Fourier transform [Fig. 1(c)], indeed, reveals two sharp features near 2000 and 2080 cm^{-1} (300 and 380 cm^{-1} in the rotating frame, respectively). Also shown in Fig. 1(c) is the linear action spectrum collected in the traditional manner by frequency-scanning a tunable, few-cm^{-1} resolution IR source (light red trace). The two methods yield essentially identical vibrational action spectra, as expected. The observation of two carbonyl stretch features is consistent with the *fac* isomer of $Re(CO)_3(CH_3CN)_3^+$ shown in Fig. 1(d). The lower-energy peak at 2000 cm^{-1} derives from a doubly degenerate pair of asymmetric stretch normal modes while the higher-energy 2080 cm^{-1} peak results from the lone symmetric stretch normal mode. The mass spectrum of $Re(CO)_3(CH_3CN)_3^+ \cdot (N_2)_n$ is presented in Fig. S1, while harmonic calculations for the *fac* and *mer* isomers are provided in Fig. S2.

To collect transient absorption spectra, a pump pulse preceding the probe pair was generated with the pulse shaper [Fig. 2(a)]. At each pump–probe waiting time T_w between the pump pulse and first probe pulse, the probe pair delay time τ was scanned and

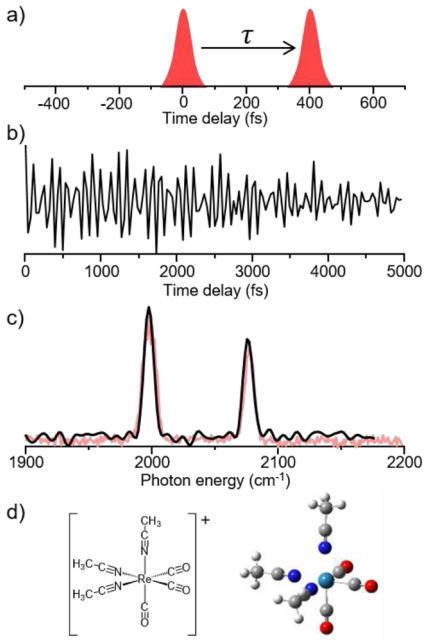

FIG. 1. (a) IR pulse pair scheme for acquisition of linear action spectra in the time domain. (b) Tag-loss interferogram of $Re(CO)_3(CH_3CN)_3^+ \cdot N_2$ undersampled with a 1700 cm^{-1} rotating frame in the carbonyl stretch region. (c) Fourier transform of the interferogram in (b) after adding the rotating frame frequency (black). The linear spectrum collected by frequency-scanning a tunable IR laser is shown in light red for comparison. (d) Structure of the *fac*-$Re(CO)_3(CH_3CN)_3^+$ isomer consistent with the measured spectrum in (c).

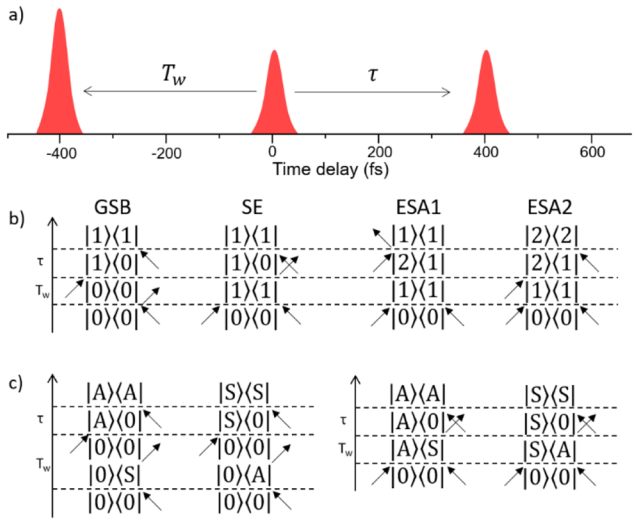

FIG. 2. (a) IR pulse scheme for acquisition of transient pump–probe spectra. (b) Feynman diagrams for the four rephasing pathways of a single-oscillator system. (c) Rephasing cross-peak bleach pathways for a coupled two-oscillator system. A = asymmetric stretch; S = symmetric stretch.

modulations in the N_2 tag-loss signal were monitored. The pulse interactions act to modulate the population in the vibrational excited states as a function of the delay times T_w and τ. The measured tag-loss signal is directly proportional to the excited vibrational population following the final pulse interaction. A potential issue using the messenger tag method is the timescale on which tag loss occurs. The tag-loss mechanism proceeds through intramolecular vibrational redistribution (IVR),[34] which will depend on the coupling between the excited vibrational modes and lower-frequency modes and, ultimately, the low-frequency ion-tag intermolecular vibrational mode. IVR typically occurs on the tens of picosecond to nanosecond timescale in the gas phase.[9–12,35–37] Tag-loss effects between the pulse delays, therefore, are not expected to contribute to the current experiments.

A major challenge in collecting nonlinear action spectra is that each pulse is capable of exciting the system individually, leading to a constant background signal. Furthermore, the interaction between a pair of pulses can contribute a linear background signal. To isolate the desired nonlinear transient absorption signal that arises from population modulation due to interactions with all three pulses, an eight-step phase cycling scheme was employed.[38] Further details on the phase cycling scheme are provided in the supplementary material. Analogous to fluorescence-modulation experiments,[17–20] modulations in the N_2 tag-loss signal were monitored as a function of the probe pair delay time τ for each phase cycling step. Representative time-domain transient tag-loss signals are presented in Fig. S3. The Fourier transform of the isolated nonlinear tag-loss modulation signal as a function of τ yields the frequency-resolved transient absorption spectrum for each pump–probe waiting time T_w.

The isolated transient absorption signal derives from eight nonlinear pathways for each normal mode, excluding possible cross-peak signals. Feynman diagrams depicting the four rephasing pathways for a single oscillator are shown in Fig. 2(b), while the four non-rephasing pathways are given in Fig. S4. Rephasing and non-rephasing pathways are indistinguishable in transient absorption experiments and are simultaneously measured to yield purely absorptive spectra. Since the measured tag-loss signal is directly proportional to the final vibrational excited-state population, only those pathways that end in an excited state (v = 1 or 2) will give rise to a tag-loss action signal.

For each pathway, there are two simultaneous interactions with the pump pulse. These interactions place the system into either the $|0\rangle\langle 0|$ or $|1\rangle\langle 1|$ population state. In the ground-state bleach (GSB) pathway, the first probe pulse interaction switches the system from $|0\rangle\langle 0|$ into the $|1\rangle\langle 0|$ coherence state. This coherence evolves during the probe pair delay time τ as $e^{-i\omega_{10}\tau}$. The second probe pulse interaction places the system into the $|1\rangle\langle 1|$ population state and modulates the excited-state population as a function of τ. The stimulated emission (SE) pathway likewise proceeds through the $|1\rangle\langle 0|$ coherence state and ends in the $|1\rangle\langle 1|$ population state. These pathways are analogous to the GSB and SE pathways (which we will collectively refer to as bleaches) in condensed-phase experiments.[2] Both bleach pathways give rise to an overall time-dependent signal that oscillates as $-e^{-i\omega_{10}\tau}$ with an intensity proportional to $|\langle 1|\mu|0\rangle|^4$. Therefore, a decrease in signal will be observed at the fundamental transition frequency ω_{10}.

The remaining two pathways are excited-state absorption (ESA) pathways, which proceed through the $|2\rangle\langle 1|$ coherence state. In contrast to typical condensed-phase experiments, the action–detection scheme results in two ESA pathways. Both ESA pathways evolve as $e^{-i\omega_{21}\tau}$ and give rise to a signal at the overtone frequency ω_{21}, with intensity proportional to $|\langle 1|\mu|0\rangle|^2|\langle 2|\mu|1\rangle|^2$.[2] Based on solution-phase experiments of metal-carbonyl complexes, overtone features would be expected to fall 10–15 cm^{-1} lower in energy than the corresponding bleach signals.[39,40] The two ESA pathways, however, oscillate at different phases. The sign of a Feynman diagram goes as $(-1)^n$, where n is the number of interactions with the bra side of the density matrix. This factor results from the nested commutators that arise from the density matrix formulation of time-dependent perturbation theory.[2,41] ESA1, therefore, oscillates as $-e^{-i\omega_{21}\tau}$, while ESA2 oscillates as $+e^{-i\omega_{21}\tau}$. Consequently, the two ESA pathways destructively interfere and cancel, leaving only bleaching signals in the nonlinear action spectra. This expectation is consistent with experimental observations by Brixner using fluorescence modulation detection in condensed-phase experiments.[42] ESA1 and ESA2 pathways were observed under certain experimental conditions by Stienkemeier using gas-phase photoionization

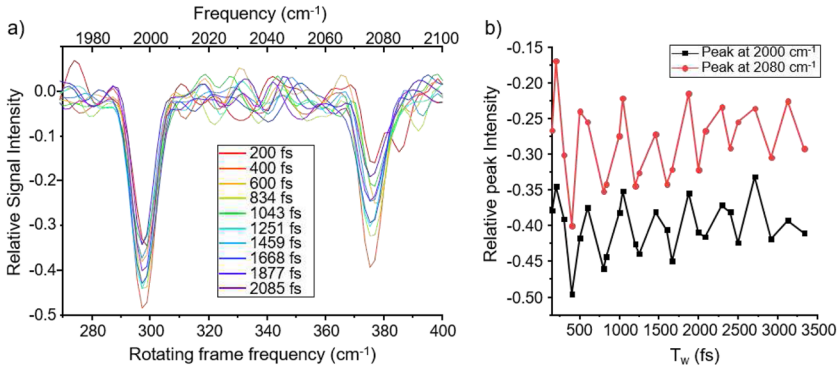

FIG. 3. (a) Transient absorption vibrational spectra of *fac*-$Re(CO)_3(CH_3CN)_3^+ \cdot N_2$ in the carbonyl stretch region at the indicated pump–probe waiting times T_w. Relatively strong bleaching signals were observed for each feature. (b) Waiting time evolution of the intensities of the two C≡O stretch bleaches at all waiting times collected. Both peaks show oscillations in intensity with a period of about 400 fs, consistent with the energy difference between the two vibrational features.

schemes.[21] In the experiments reported here, only bleaching signals are expected since equal tag loss is expected regardless of the final population state of the system ($|1\rangle\langle 1|$ or $|2\rangle\langle 2|$; i.e., the N_2 binding energy is $\ll\hbar\omega_{10}$).

Transient absorption spectra of *fac*-$Re(CO)_3(CH_3CN)_3^+ \cdot N_2$ at several selected waiting times T_w are presented in Fig. 3(a). For all spectra presented, the pump pulse was set to have twice the amplitude compared to the individual probe pulses. Power-dependence measurements confirmed that transient signals were linear in pump power (Fig. S5). Relatively strong bleaching signals were observed at the fundamental frequencies of the two normal modes. The total change in photodissociation yield compared to the linear response was around −15%, as measured from the raw time-domain data. Each frequency-resolved spectrum presented in Fig. 3 was normalized to its respective frequency-resolved linear spectrum, which was simultaneously collected, to account for ion signal fluctuations between scans. Details about data processing procedures are provided in the supplementary material. The large nonlinear signals are not surprising given the very strong oscillator strengths of carbonyl stretches in metal complexes. As expected, ESA signals are not observed at the overtone frequencies.

Excitingly, the bleach signals from both features oscillate with pump–probe waiting time with a period of ~400 fs. This oscillation period is consistent with the difference frequency between the two vibrational peaks (80 cm^{-1}, 417 fs). This observation suggests the presence of coherent coupling between the symmetric and asymmetric carbonyl stretch pair. Metal-carbonyl complexes have been well characterized in the condensed phase using ultrafast transient and 2D IR spectroscopies.[3,39,40,43–48] Symmetric and asymmetric carbonyl stretch pairs in these systems yield relatively strong off-diagonal cross-peak signals. In transient absorption experiments, where only the probe axis is resolved, the measured signals are the sum of the contributions from the diagonal pathways depicted in Fig. 2(b) and those from the cross-peak pathways. Rephasing cross-peak bleach pathways for a coupled two-oscillator system are depicted in Fig. 2(c), with the complete set of pathways given in Fig. S6. Numerous cross-peak pathways involve states $|A\rangle\langle S|$ during the waiting time T_w, where A denotes asymmetric stretch and S denotes symmetric stretch, respectively. These states are generated by the pump interactions, where the first pump interaction excites the asymmetric stretch and the second pump interaction excites the symmetric stretch, or vice versa.[2] During the waiting time T_w, these states evolve at the difference frequency ω_{AS} between the coupled oscillators, $e^{-i\omega_{AS}T_w}$. Indeed, strong oscillations with periods of $1/2\pi\omega_{AS}$ have been reported in the condensed-phase transient and 2D IR spectra of metal-carbonyl complexes.[39,44,45]

The intensity evolution of the two C≡O peaks across all waiting times collected is presented in Fig. 3(b). Importantly, the largest signal modulations were observed at pump–probe waiting times T_w corresponding to the expected 417 fs period. This observation confirms that the recorded N_2 tag-loss action signals derive from nonlinear pathways and that underlying cross-peak signals are present. We note that the cross-peaks in *fac*-$Re(CO)_3(CH_3CN)_3^+$ are expected to be much stronger in the ZZYY polarization scheme[3,46,47] (when pump and probe pulses have perpendicular polarizations) since the symmetric and asymmetric carbonyl stretches have orthogonal transition moments. The current setup, however, is limited to the ZZZZ (parallel polarization) scheme. The bleach signals also appear to show a small overall decay in signal with waiting time T_w. In non-polar solvents, carbonyl stretches in metal complexes exhibit very long vibrational lifetimes (10s ps).[44,48] With no solvent present in the gas phase (except for the single N_2 tag) and very few low-frequency modes to couple to, the bleach signals for *fac*-$Re(CO)_3(CH_3CN)_3^+$ are expected to show minimal decay dynamics throughout the measured waiting time series. Without solvent, the ground state of isolated molecular ions will never be repopulated and the ions will remain vibrationally hot following excitation. Shifts in vibrational frequencies might be observed in species where transitions exist that are highly sensitive to the excitation of lower-frequency modes via IVR. ESA transitions would be the direct and ideal reporters of vibrational lifetime dynamics. Given that the ESA2 pathway ends in the $|2\rangle\langle 2|$ population state while all other pathways end in $|1\rangle\langle 1|$, this path could be isolated if a strong-binding tag or a multiple tag-loss mass channel is utilized which requires energy greater than $\hbar\omega_{10}$ to occur. Measured vibrational dynamics are also limited to the tag-loss timescale. Given typical IVR timescales,[9–12,35–37] interesting vibrational dynamics should still be accessible using the tag-loss method. One intriguing possibility is to measure rotational reorientation dynamics as a method for elucidating the structures of large molecular systems.[49]

IV. SUMMARY

We have presented a successful demonstration of frequency-resolved ultrafast transient vibrational action spectroscopy on cryogenically cooled *fac*-$Re(CO)_3(CH_3CN)_3^+$ ions. Although the very intense carbonyl stretch features in the metal complex provided an ideal test system, the scheme is generally applicable. As another example, the transient absorption spectrum of protonated caffeine ($C_8H_{10}N_4O_2H^+$) in the fingerprint region is presented in Fig. S7. The current demonstration also lays the foundations for the acquisition of 2D IR and transient UV/Vis–IR spectra on dilute molecular ion ensembles, which could be highly impactful tools for the study of chemical structures and reaction dynamics. The general strategies presented here can also be applied to dilute neutral systems. For neutrals, an additional UV/Vis pulse is required to generate an action response, such as photofragmentation or ionization, that is modulated by the preceding IR pulse sequence.

Future 2D IR experiments will reveal critical cross-peaks that encode intra- and intermolecular couplings and interactions. Here, the absence of ESA signals will be beneficial for resolving cross-peaks within congested spectral regions. 2D experiments will require a pump pulse pair to resolve the excitation axis via a two-dimensional Fourier transform over the pump and probe pair time delays. Alternative data collection schemes, such as sparse sampling,[50–54] will be necessary to reduce the total time needed to obtain a spectrum. Alternatively, scanning a frequency-resolved picosecond pump pulse might provide a better approach for resolving the excitation axis if sub-ps time resolution is not required.[55,56] For transient UV/Vis–IR spectroscopy, electronic excitation with a UV/Vis pulse to initiate a reactive process should result in larger changes in the IR spectra that evolve more discernibly as a reaction proceeds on excited electronic potential energy surfaces. An additional benefit here is that fewer phase cycling steps are required with a

non-IR pump pulse to isolate the transient signal. Overall, transient and 2D spectroscopies on isolated molecular ion systems will play an important new role in unraveling reaction mechanisms at the molecular level, which are often too difficult to elucidate with current condensed-phase methodologies, particularly for electron and proton transfer reactions.

SUPPLEMENTARY MATERIAL

Experimental details on ion generation, pulse generation, data acquisition, and data processing; mass spectrum of $Re(CO)_3(CH_3CN)_3^+ \cdot (N_2)_n$ (Fig. S1); harmonic calculations of the *fac* and *mer* isomers of $Re(CO)_3(CH_3CN)_3^+$ (Fig. S2); representative time-domain tag-loss signal for transient absorption experiments (Fig. S3); non-rephasing pathways of a single oscillator system (Fig. S4); pump pulse power dependence (Fig. S5); all rephasing and non-rephasing pathways for a two-oscillator system (Fig. S6); and transient action spectrum of protonated caffeine (Fig. S7).

ACKNOWLEDGMENTS

J.A.F. gratefully acknowledges the support from NSF through a CAREER Award (Grant No. CHE-2044927).

AUTHOR DECLARATIONS

Conflict of Interest

The authors have no conflicts to disclose.

Author Contributions

L.C. and Z.M. contributed equally to this work.

Liangyi Chen: Data curation (equal); Formal analysis (equal); Investigation (equal); Methodology (equal); Validation (equal); Visualization (equal); Writing – original draft (supporting); Writing – review & editing (supporting). **Zifan Ma**: Data curation (equal); Formal analysis (equal); Investigation (equal); Methodology (equal); Validation (equal); Visualization (equal); Writing – original draft (supporting); Writing – review & editing (supporting). **Joseph A. Fournier**: Conceptualization (lead); Data curation (equal); Formal analysis (equal); Funding acquisition (lead); Investigation (supporting); Methodology (supporting); Project administration (lead); Supervision (lead); Validation (equal); Visualization (supporting); Writing – original draft (lead); Writing – review & editing (lead).

DATA AVAILABILITY

The data that support the findings of this study are available from the corresponding author upon reasonable request.

REFERENCES

[1] P. Hamm and A. Shalit, J. Chem. Phys. **146**, 130901 (2017).
[2] P. Hamm and M. Zanni, *Concepts and Methods of 2D Infrared Spectroscopy* (Cambridge University Press, 2011).
[3] M. Khalil, N. Demirdöven, and A. Tokmakoff, J. Phys. Chem. A **107**, 5258 (2003).
[4] J. D. Hybl, A. W. Albrecht, S. M. Gallagher Faeder, and D. M. Jonas, Chem. Phys. Lett. **297**, 307 (1998).
[5] J. D. Hybl, A. Albrecht Ferro, and D. M. Jonas, J. Chem. Phys. **115**, 6606 (2001).
[6] T. L. Courtney, Z. W. Fox, L. Estergreen, and M. Khalil, J. Phys. Chem. Lett. **6**, 1286 (2015).
[7] T. A. A. Oliver, N. H. C. Lewis, and G. R. Fleming, Proc. Natl. Acad. Sci. U. S. A. **111**, 10061 (2014).
[8] B. I. Grimberg, V. V. Lozovoy, M. Dantus, and S. Mukamel, J. Phys. Chem. A **106**, 697 (2002).
[9] H. S. Yoo, M. J. DeWitt, and B. H. Pate, J. Phys. Chem. A **108**, 1348 (2004).
[10] H. S. Yoo, M. J. DeWitt, and B. H. Pate, J. Phys. Chem. A **108**, 1365 (2004).
[11] H. S. Yoo, D. A. McWhorter, and B. H. Pate, J. Phys. Chem. A **108**, 1380 (2004).
[12] S. T. Shipman, P. C. Douglass, H. S. Yoo, C. E. Hinkle, E. L. Mierzejewski, and B. H. Pate, Phys. Chem. Chem. Phys. **9**, 4572 (2007).
[13] C. Schriever, S. Lochbrunner, E. Riedle, and D. J. Nesbitt, Rev. Sci. Instrum. **79**, 13107 (2008).
[14] A. Mandal, G. Ng Pack, P. P. Shah, S. Erramilli, and L. D. Ziegler, Phys. Rev. Lett. **120**, 103401 (2018).
[15] N. C. Cole-Filipiak, J. Troß, P. Schrader, L. M. McCaslin, and K. Ramasesha, J. Chem. Phys. **154**, 134308 (2021).
[16] N. C. Cole-Filipiak, J. Troß, P. Schrader, L. M. McCaslin, and K. Ramasesha, J. Chem. Phys. **156**, 144306 (2022).
[17] P. F. Tekavec, T. R. Dyke, and A. H. Marcus, J. Chem. Phys. **125**, 194303 (2006).
[18] P. F. Tekavec, G. A. Lott, and A. H. Marcus, J. Chem. Phys. **127**, 214307 (2007).
[19] S. Roeding and T. Brixner, Nat. Commun. **9**, 2519 (2018).
[20] H.-P. Solowan, P. Malý, and T. Brixner, J. Chem. Phys. **157**, 044201 (2022).
[21] L. Bruder, U. Bangert, M. Binz, D. Uhl, R. Vexiau, N. Bouloufa-Maafa, O. Dulieu, and F. Stienkemeier, Nat. Commun. **9**, 4823 (2018).
[22] L. Bruder, U. Bangert, M. Binz, D. Uhl, and F. Stienkemeier, J. Phys. B: At., Mol. Opt. Phys. **52**, 183501 (2019).
[23] M. A. R. Reber, Y. Chen, and T. K. Allison, Optica **3**, 311 (2016).
[24] M. C. Silfies, G. Kowzan, N. Lewis, and T. K. Allison, Phys. Chem. Chem. Phys. **23**, 9743 (2021).
[25] L. Guyon, T. Tabarin, B. Thuillier, R. Antoine, M. Broyer, V. Boutou, J.-P. Wolf, and P. Dugourd, J. Chem. Phys. **128**, 02B624 (2008).
[26] L. MacAleese, S. Hermelin, K. E. Hage, P. Chouzenoux, A. Kulesza, R. Antoine, L. Bonacina, M. Meuwly, J.-P. Wolf, and P. Dugourd, J. Am. Chem. Soc. **138**, 4401 (2016).
[27] S. J. P. Marlton, B. I. McKinnon, P. Greißel, O. J. Shiels, B. Ucur, and A. J. Trevitt, J. Chem. Phys. **155**, 184302 (2021).
[28] L. Chen, J. L. S. Dean, and J. A. Fournier, J. Phys. Chem. A **125**, 10235 (2021).
[29] M. Okumura, L. I. Yeh, J. D. Myers, and Y. T. Lee, J. Chem. Phys. **85**, 2328 (1986).
[30] B. M. Marsh, J. M. Voss, and E. Garand, J. Chem. Phys. **143**, 204201 (2015).
[31] J. J. Kreinbihl, N. C. Frederiks, and C. J. Johnson, J. Chem. Phys. **154**, 014304 (2021).
[32] N. Heine and K. R. Asmis, Int. Rev. Phys. Chem. **34**, 1 (2015).
[33] A. B. Wolk, C. M. Leavitt, E. Garand, and M. A. Johnson, Acc. Chem. Res. **47**, 202 (2014).
[34] D. J. Nesbitt and R. W. Field, J. Phys. Chem. **100**, 12735 (1996).
[35] V. B. Laptev, V. O. Kompanets, S. V. Pigulsky, A. A. Makarov, G. V. Mishakov, D. V. Serebryakov, A. V. Sharkov, S. V. Chekalin, and E. A. Ryabov, J. Phys. Chem. A **123**, 771 (2019).
[36] S. V. Chekalin, V. O. Kompanets, P. V. Koshlyakov, V. B. Laptev, S. V. Pigulsky, A. A. Makarov, and E. A. Ryabov, J. Phys. Chem. A **118**, 955 (2014).
[37] C. Stromberg, D. J. Myers, and M. D. Fayer, J. Chem. Phys. **116**, 3540 (2002).
[38] H.-S. Tan, J. Chem. Phys. **129**, 124501 (2008).
[39] O. Golonzka, M. Khalil, N. Demirdöven, and A. Tokmakoff, J. Chem. Phys. **115**, 10814 (2001).
[40] C. R. Baiz, P. L. McRobbie, J. M. Anna, E. Geva, and K. J. Kubarych, Acc. Chem. Res. **42**, 1395 (2009).
[41] S. Mukamel, *Principles of Nonlinear Optical Spectroscopy* (Oxford University Press, 1995).

[42]P. Malý and T. Brixner, Angew. Chem., Int. Ed. **60**, 18867 (2021).
[43]L. M. Kiefer and K. J. Kubarych, Coord. Chem. Rev. **372**, 153 (2018).
[44]J. T. King, C. R. Baiz, and K. J. Kubarych, J. Phys. Chem. A **114**, 10590 (2010).
[45]L. M. Kiefer, J. T. King, and K. J. Kubarych, J. Phys. Chem. A **118**, 9853 (2014).
[46]C. S. Peng, K. C. Jones, and A. Tokmakoff, J. Am. Chem. Soc. **133**, 15650 (2011).
[47]L. P. DeFlores, R. A. Nicodemus, and A. Tokmakoff, Opt. Lett. **32**, 2966 (2007).
[48]L. M. Kiefer and K. J. Kubarych, J. Phys. Chem. A **119**, 959 (2015).
[49]T. F. Magnera, D. M. Sammond, and J. Michl, Chem. Phys. Lett. **211**, 378 (1993).
[50]J. C. J. Barna, E. D. Laue, M. R. Mayger, J. Skilling, and S. J. P. Worrall, J. Magn. Reson. **73**, 69 (1987).
[51]J. C. Hoch, M. W. Maciejewski, and B. Filipovic, J. Magn. Reson. **193**, 317 (2008).
[52]J. A. Dunbar, D. G. Osborne, J. M. Anna, and K. J. Kubarych, J. Phys. Chem. Lett. **4**, 2489 (2013).
[53]J. N. Sanders, S. K. Saikin, S. Mostame, X. Andrade, J. R. Widom, A. H. Marcus, and A. Aspuru-Guzik, J. Phys. Chem. Lett. **3**, 2697 (2012).
[54]I. Bhattacharya, J. J. Humston, C. M. Cheatum, and M. Jacob, Opt. Lett. **42**, 4573 (2017).
[55]P. Hamm, M. Lim, and R. M. Hochstrasser, J. Phys. Chem. B **102**, 6123 (1998).
[56]P. Hamm, M. Lim, W. F. DeGrado, and R. M. Hochstrasser, Proc. Natl. Acad. Sci. U. S. A. **96**, 2036 (1999).